Available online at www.sciencedirect.com
SCIENCE DIRECT®
International Journal of Heat and Mass Transfer 49 (2006) 317–328
International Journal of HEAT and MASS TRANSFER
www.elsevier.com/locate/ijhmt

An estimation of effective thermal conductivity of a fibrous dual-scale porous medium during unsaturated flow

Murthy S. Munagavalasa [a], Krishna M. Pillai [b,*]

[a] S.C. Johnson and Son, Inc., 1525 Howe Street, Racine, WI 53403, USA
[b] Department of Mechanical Engineering, University of Wisconsin-Milwaukee, 945 EMS Building, 3200 N. Cramer Street, Milwaukee, WI 53211, USA

Received 2 December 2004; received in revised form 22 June 2005
Available online 24 August 2005

Abstract

The effective thermal conductivity in the volume-averaged temperature equation for the dual-scale porous media is estimated numerically. A finite-element simulation of a steady Newtonian flow in the unit cell of an idealized dual-scale porous medium is carried out and the relevant component of the effective thermal conductivity tensor is estimated from the resultant temperature and velocity fields. It is discovered that the conductivity is a strong function of Péclet number as well as inter-tow spacing, but is insensitive to the rate of tow wetting or the heat-flux from tows. We also conclude that the conductivity remains unchanged in the saturated as well as unsaturated flow regimes in dual-scale porous media.

1. Introduction

Heat transfer during transport of liquid through porous media is important in the manufacture of polymeric composites. In liquid composite molding (LCM) processes such as resin transfer molding (RTM), a room-temperature thermoset resin in the form of a viscous Newtonian liquid is injected into a closed hot mold containing reinforcements such as carbon or glass fibers [1]. The temperature distribution is affected by thermal conduction through fibers and resin, as well as thermal convection due to fluid motion. An accurate prediction of temperature distribution is important in order to facilitate the optimization of LCM mold design as the resin flow during the mold-filling simulations is affected by resin viscosity, which in turn is a strong function of temperature and degree of cure.

A porous medium where all pores are of the same length-scale, is conventionally referred to as a single-scale porous medium. An LCM mold containing randomly oriented fibers of a random mat is an example of the single-scale porous medium. The fibers are impermeable and the spacing between fibers can be treated as homogeneous. However, if the solid phase is porous with the pore size of a much smaller length-scale, the porous medium is then classified as a dual length-scale or dual porosity porous medium. Braided, woven or stitched fiber mats used in LCM processes, where fiber bundles are permeable to resin due to presence of pores between fibers within the bundles, fall under this category. The transport processes that occur inside this dual-scale porous medium are often significantly

* Corresponding author. Tel.: +1 414 229 6535.
E-mail address: krishna@uwm.edu (K.M. Pillai).

0017-9310/$ - see front matter © 2005 Elsevier Ltd. All rights reserved.
doi:10.1016/j.ijheatmasstransfer.2005.06.020

Nomenclature

A	area inside representative elementary volume (REV)
$\hat{B}$	local deviation in B from its gap average ($\hat{B} = B - \langle B\rangle^{g}$)
$\mathbf{b}$, b_i	a vector field that relates local temperature fluctuations to the gradient of gap-averaged temperature (i.e. $\hat{T}_g = \mathbf{b}\cdot\nabla\langle T_g\rangle^{g}$)
C_p	constant pressure specific heat
f_c	reaction rate
$\mathbf{g}$	acceleration due to gravity
H_R	heat of reaction per unit mass
k	thermal conductivity
$\mathbf{K}$	permeability tensor
$\mathbf{K}_{th}$	effective thermal conductivity tensor
$K_{th,ij}$	i, j component of the effective thermal conductivity tensor
$\mathbf{n}_{gt}$	unit normal vector at the gap–tow interface pointing from gap phase to tow phase
P	pressure
$\mathbf{q}$	conductive heat-flux
S	sink strength (rate of resin absorption by tows per unit volume)
s	width and height of periodic unit cell
T	temperature
$\mathbf{v}$	velocity
V	volume within REV
x, y, z	Cartesian coordinates

Greek symbols

$\boldsymbol{\delta}$, δ_{ij}	Kronecker delta
ρ	density of resin
μ	viscosity of resin
ε	porosity

Subscripts

g	pertaining to gap phase
t	pertaining to tow phase
gt	pertaining to gap–tow interface
i	take values x, y and z
j	take values x, y and z

Superscript

*	dimensionless quantity

Others

$\langle\rangle$	volume average
$\langle\rangle^{g}$	gap average
$\langle\rangle^{gt}$	average over the gap–tow interface
$\{\}_{in}$	surface averaging operator over the inlet gap area
$\{\}_{out}$	surface averaging operator over the outlet gap area
∇	gradient operator

different from that of the single-scale porous medium. Babu and Pillai [2] discovered that the dual-scale porous media with continuous inter-tow gaps[1] (created by the stitched mats only) allow the lead-lag flow to manifest where the resin races along the gaps before fully impregnating the tows.[2] A schematic showing such a flow is included in Fig. 1 where the delayed wetting of tows behind the resin front in the gap region leads to a region of partial saturation behind the front in such dual-scale fiber mats. The flow in such a region is called the *unsaturated* flow and is often characterized either by a visually observable region of a lighter hue as compared to the darker saturated region (Fig. 2), or by a droop in the inlet-pressure history [2].

The mathematically rigorous volume averaging method developed by Whitaker et al. [3–11] offers a simplified alternative to solving the pointwise governing equations in complex pore space of the fibrous porous medium created in the LCM mold; the method yields a set of governing equations in averaged variables that are solved numerically over the porous medium to predict the non-isothermal transport of a reactive resin during the mold-filling process. In the past, the volume averaging methods have been successfully used in deriving transport equations for single-phase flow in the single-scale porous media [3–9] and were later adapted to the dual-scale fractured porous media [3,10,11]. Using these methods, Pillai and Munagavalasa [12,13] derived the mathematically rigorous transport equations for reactive non-isothermal flow in a dual-scale porous medium as applicable to predicting the LCM mold-filling process. A characteristic feature of these equations is the presence of several source and sink terms in the mass, energy and chemical species equations.

The objective of this paper is to study variations in the effective thermal conductivity, a very important parameter in the newly derived temperature equation that governs the redistribution of energy, during the unsaturated flow. One issue that we would like to explore is the effect of resin absorption by tows in a dual-scale porous medium (which leads to a 'sink' term or a negative source term in the mass balance equation)

[1] Large-scale pores between tows will be referred to as the gap phase or gap region, or just gaps.

[2] Fiber bundles will be referred to as the tow phase or tow region, or just tows.

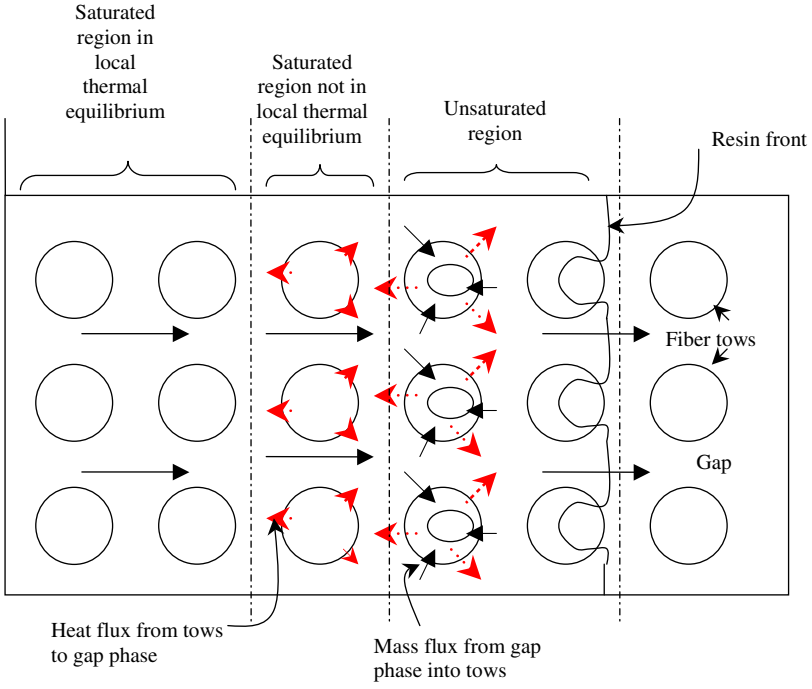

Fig. 1. A schematic describing various flow regimes in a dual-scale porous medium. The unsaturated region is immediately behind the flow front followed first by the saturated region that is not in local thermal equilibrium and then by the saturated region where the tow and gap phases are in thermal equilibrium.

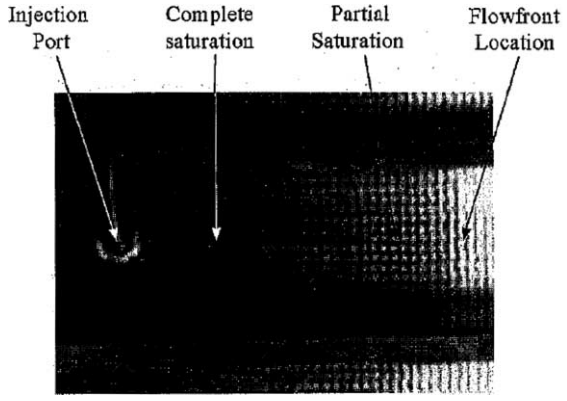

Fig. 2. Appearance of unsaturated flow region behind the flow front during a point injection in a woven fiber mat. Regular pattern of dark and light spots in the unsaturated or partially saturated region is due to periodicity in the structure of the mat.

on the effective thermal conductivity tensor. This will enable us to chart variations in the tensor as tows start delayed resin absorption behind the flow front and gradually reaches fully steady-state condition during the LCM mold-filling process in dual-scale fiber mats.

The organization of the paper is as follows. In Section 1, a brief description of the volume averaging method and a synopsis of the relevant volume-averaged equations for the dual-scale porous media is presented. In Section 2, we describe how the numerical simulation of a steady-state, non-isothermal, 2D flow in the unit cell of a dual-scale medium is employed to estimate the relevant component of effective thermal conductivity tensor. Later in Section 3, we describe the results of this estimation in the form of a parametric study. In Section 4, conclusions and limitations of the study are presented.

1.1. Volume averaging method adapted to the dual-scale porous media

The volume averaging method is applied to the single-phase flow in a single-scale porous medium to derive the balance equations at the macroscopic level by using the balance equations for various physical quantities at the microscopic level [3–9]. The medium is divided into two phases, solid and liquid, and flow variables are averaged over an averaging volume which is much bigger than the individual pores and particles.

We adapted the volume averaging method to the dual-scale porous medium created by the woven, stitched or braided fiber mats in LCM where the two 'phases' considered were the porous fiber-tows and the surrounding gaps [12,13]. The tows, unlike the solid phase in single-scale porous medium, consist of liquid,

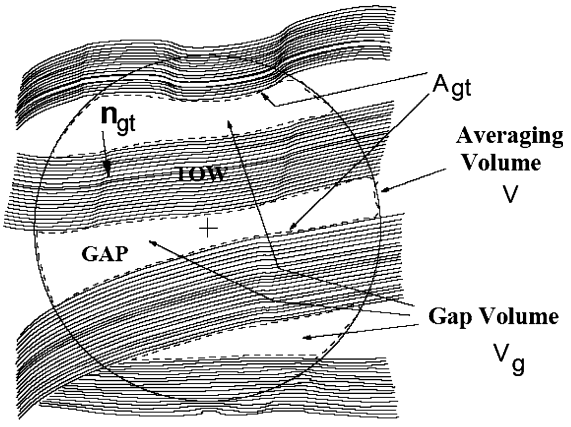

Fig. 3. Representative elementary volume for a fibrous dual-scale porous medium.

solid and air[3] phases whereas the gaps are filled entirely with the liquid phase. Fig. 3 describes an averaging volume for a fibrous dual-scale medium. Since the dual-scale fibrous media such as woven or stitched fiber mats are often periodic, the size of averaging volume can be reduced from being much larger than the thickness of tows to a unit cell of such a periodic medium.

The volume average $\langle B_g \rangle$ of quantity B_g averaged over the averaging volume[4] is defined as

$$\langle B_g \rangle = \frac{1}{V}\int_{V_g} B_g \, dV \tag{1}$$

where V_g is the volume of gap region within the averaging volume of volume V as shown in Fig. 3. The volume average $\langle B_g \rangle$ is related to the gap average as

$$\langle B_g \rangle = \varepsilon_g \langle B_g \rangle^g \tag{2}$$

where ε_g the gap fraction is defined as $\varepsilon_g = V_g/V$.

1.2. Summary of volume-averaged transport equations

Pillai and Munagavalasa [12,13] rigorously derived the macroscopic transport equations for the dual-scale porous media using the volume averaging method, the summary of which is presented in this section. Only the relevant gap-averaged balance laws will be listed; their derivation as well as the estimation of their various source and sink terms with the help of the single-scale model for the intra-tow flows is presented elsewhere [12,13].

Macroscopic mass balance equation is given as

$$\nabla \cdot \langle \mathbf{v}_g \rangle = -S \tag{3}$$

where S is the (mass) sink term and is equal to the volumetric rate of absorption of resin by the tows per unit volume:

$$S = \frac{1}{V}\int_{A_{gt}} \mathbf{v}_g \cdot \mathbf{n}_{gt} \, dA \tag{4}$$

The minus sign of the sink term in the continuity equation suggests that the flow of the resin slows down in the unsaturated gap region because of the absorption of the resin by the tows. An estimation of S requires the integration of resin flux into the tows, which in turn require solving the single-scale transport equations within the tow region [13,16].

When the inertial and gravitational effects along with sharp gradients in the sink term S can be neglected, the macroscopic momentum balance equation for the gap region simplifies to the well known Darcy's law:

$$\langle \mathbf{v}_g \rangle = \frac{\mathbf{K}}{\mu_g} \cdot \nabla \langle P_g \rangle^g \tag{5}$$

The gap-averaged energy balance equation is given as

$$\rho_g C_{p,g} \left\{ \varepsilon_g \frac{\partial}{\partial t} \langle T_g \rangle^g + \langle \mathbf{v}_g \rangle \cdot \nabla \cdot \langle T_g \rangle^g \right\} = \nabla \cdot \mathbf{K}_{th} \cdot \nabla \langle T_g \rangle^g + \varepsilon_g \rho_g H_R f_c + Q_{conv} - Q_{cond} \tag{6}$$

where $\mathbf{K}_{th}$ is the effective thermal conductivity tensor for the dual-scale porous media and is given as

$$\mathbf{K}_{th} = k_g \varepsilon_g \boldsymbol{\delta} + \frac{k_g}{V}\int_{A_{gt}} \mathbf{n}_{gt}\mathbf{b} \, dA - \frac{\rho_g C_{p,g} \varepsilon_g}{V_g}\int_{V_g} \hat{\mathbf{v}}_g \mathbf{b} \, dV \tag{7}$$

where $\hat{\mathbf{v}}_g$ is the deviation of $\mathbf{v}_g$ from its gap-averaged value ($\hat{\mathbf{v}}_g = \mathbf{v}_g - \langle \mathbf{v}_g \rangle^g$); $\mathbf{b}$ is the vector function that transforms the gradient of the gap-averaged temperature into the local variations of the temperature deviation as $\hat{T}_g = \mathbf{b} \cdot \nabla \langle T_g \rangle^g$. Q_{conv} is the heat source term caused by the release of resin heat prior to the absorption of gap resin by the surrounding tows and is given as

$$Q_{conv} = \rho_g C_{p,g} S \lfloor \langle T_g \rangle^g - \langle T_g \rangle^{gt} \rfloor \tag{8}$$

The heat sink term created by the conductive heat loss to tows, Q_{cond}, is given as

$$Q_{cond} = \frac{1}{V}\int_{A_{gt}} \mathbf{q}_g \cdot \mathbf{n}_{gt} \, dA \tag{9}$$

Incidentally, both Q_{conv} and Q_{cond} will be negative for the case of a cold resin invading into a pre-warmed LCM mold. In addition, either empirical correlations

[3] Ideally, the air phase would be replaced by vacuum 'phase'—the proposed theory is exactly true if the interstitial spaces in a dual-scale porous medium is a vacuum. (It prevents the formation of air-bubbles inside tows and avoids the accompanying complications of a two-phase flow in the porous medium.)

[4] Often referred to as the representative elementary volume (REV) as well.

or microscopic calculations will be needed to estimate $\mathbf{K}_{th}$, Q_{conv} and Q_{cond} during the unsaturated and saturated flow regimes in a dual-scale porous medium.

2. Effective thermal conductivity tensor

In order to solve the macroscopic energy equations, one needs to evaluate the effective thermal conductivity $\mathbf{K}_{th}$ before hand. The effective thermal conductivity tensor given by Eq. (7) comprises of two parts: a molecular diffusion part (the first two terms on the RHS of Eq. (7)) and a hydrodynamic dispersion[5] part (the third term on the RHS of Eq. (7)). One requires to know **b** distribution (or indirectly $\widehat{T}_g$ distribution) in an averaging volume to estimate the former, and both **b** and $\hat{\mathbf{v}}_g$ distributions to estimate the latter. It is important to realize that the **b** field is also a function of pointwise velocity deviations. The pointwise velocity deviations can be obtained by solving the microscopic momentum balance equation in the gap phase. Kaviany [4] provides an excellent summary of available correlations for the phase-averaged effective thermal conductivity for single-scale porous media with periodic unit cells. Hsiao and Advani [14] numerically evaluate the dependency of the phase-averaged effective thermal conductivity term on Péclet number, Reynolds number, ratio of thermal conductivities of the solid and fluid, porosity of the gap and pore structure of periodic single-scale porous media. However, their studies are confined to single-scale porous media where the solid and liquid phases are in local thermal equilibrium. *So far, we have not come across any research on evaluating the effective thermal conductivity in dual-scale porous media during the unsaturated flow where the gap and tow phases are exchanging energy in the form of heat while the gap liquid is being absorbed into tows.*

So our objective in this paper is to evaluate the effect of (1) the liquid absorption rate into tows (proportional to the sink term S given by Eq. (4)), and (2) the conductive heat release rate from tows (proportional to the conductive heat sink term Q_{cond} given by Eq. (9)), on the effective thermal conductivity $\mathbf{K}_{th}$.

2.1. Dimensionless equations for flow modeling

In order to estimate $\mathbf{K}_{th}$ for the dual-scale porous media, we plan to solve the pointwise fluid motion and temperature equations in an idealized dual-scale porous medium under the unsaturated flow conditions. Consider the flow of resin along x direction in an idealized geometry of a dual-scale porous medium as shown in Fig. 4.

[5] The hydrodynamic dispersion part refer to the enhancement of heat transfer due to the local fluctuations in resin velocity within an averaging volume.

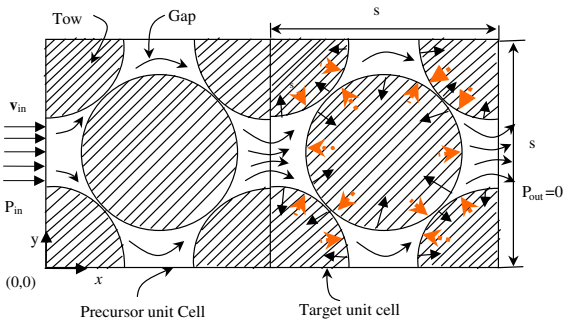

Fig. 4. A Schematic illustrating the precursor and target unit cells used in numerical simulations.

The porous medium is periodic and hence can be analyzed in terms of unit cells. The target unit cell is selected in an array of infinitely long cylindrical tows whose axes are oriented along the z direction and are periodically arranged in the x–y plane. The flow is taking place from left to right, and the macroscopic temperature gradient is applied in the same direction as well. We intend to create a steady-state non-isothermal flow in the unit cell such that the $y = s/2$ plane passing through the center of the middle cylindrical tow is the plane of symmetry.

In order to render the equations dimensionless, as well as to present the results in dimensionless form, the following characteristic quantities are chosen: unit cell width s as characteristic length, $\{v_{g,x}\}_{in}$ as characteristic velocity, and k_g as the characteristic thermal conductivity. The dimensionless temperature is defined as $T^* = \frac{T-\{T_g\}_{in}}{T_{mold}-\{T_g\}_{in}}$. At low Reynolds number, dimensionless pressure is defined as $P^* = \frac{P}{\rho_g\{\mathbf{v}_g\}_{in}^2}$.

When the physical properties of the resin and tow fibers are assumed to be constant, gravitational forces to be negligible, and the flow to be non-reactive, the dimensionless microscopic transport equations are as follows.

The dimensionless mass balance equation is

$$\nabla \cdot \mathbf{v}_g^* = 0 \tag{10}$$

The dimensionless momentum balance equation is

$$\mathbf{v}_g^* \cdot \nabla^* \mathbf{v}_g^* = -\nabla^* P^* + \mu_g^* \nabla^{*2} \mathbf{v}_g^* \tag{11}$$

The dimensionless viscosity is defined as $\mu_g^* = \frac{1}{Re}$ where $Re = \frac{\rho_g\{v_{g,x}\}_{in}s}{\mu_g}$ is the Reynolds number.

The dimensionless energy balance equation is

$$C_{p,g}^* \mathbf{v}_g^* \cdot \nabla^* T_g^* = -\nabla^{*2} T_g^* \tag{12}$$

The dimensionless specific heat is defined as $C_{p,g}^* = Pe = \frac{\rho_g\{v_{g,x}\}_{in}sC_{p,g}}{k_g}$ where Pe is the Péclet number.

If the velocity at the tow–gap interface $\mathbf{v}_g|_{gt} \cdot \mathbf{n}_{gt}$ is expressed as characteristic velocity $\{v_{g,x}\}_{in}$ multiplied by some constant, the boundary condition for the momentum balance equation at the tow–gap interface becomes

$$\mathbf{v}^*_{\mathrm{g}}|_{gt} \cdot \mathbf{n}_{gt} = \frac{\mathbf{v}_{\mathrm{g}}|_{\mathrm{gt}} \cdot \mathbf{n}_{\mathrm{gt}}}{\{v_{\mathrm{g},x}\}_{\mathrm{in}}} = \text{const.} \tag{13}$$

Similarly, the energy flux boundary condition at tow–gap interface can be assumed to a constant. This gives rise to the following boundary condition for the microscopic energy equation.

$$\mathbf{q}^*_{\mathrm{gt}} \cdot \mathbf{n}_{\mathrm{gt}} = \text{const.} \tag{14}$$

(Note that the normal velocity and conductive heat-flux at tow–gap interface are not constant, and are functions of resin flow and temperature distribution inside tows [13,16,17]. We will be using them as parameters in our simulations so as to estimate the bounds of $K_{\mathrm{th},ij}$ in the unsaturated region.)

The temperature gradient is estimated using the surface-averaged temperatures as

$$\frac{\partial\left\langle T^*_{\mathrm{g}}\right\rangle^{\mathrm{g}}}{\partial x^*} = \left\{T^*_{\mathrm{g}}\right\}_{\mathrm{out}} - \left\{T^*_{\mathrm{g}}\right\}_{\mathrm{in}} \tag{15}$$

Table 1
Typical parameter values used during the numerical simulations

Dimensional parameter	Value	Dimensionless parameter	Value
$C_{p,\mathrm{g}}$	1316 J/kg K	$C^*_{p,g}(= Pe)$	71.08–7108
k_{g}	0.16 W/m K	k^*_{g}	1
k_{s}	8.70 W/m K	k^*_{s}	54.375
$\{P_{\mathrm{g}}\}_{\mathrm{out}}$	0	$\{P^*_{\mathrm{g}}\}_{\mathrm{out}}$	0
$-\mathbf{q}_{\mathrm{g}}\|_{\mathrm{gt}} \cdot \mathbf{n}_{\mathrm{gt}}$	1.5–150 W/m^2	$-\mathbf{q}^*_{\mathrm{g}}\|_{\mathrm{gt}} \cdot \mathbf{n}_{\mathrm{gt}}$	0.322–32.2
r_{t}	0.00275 m	r^*_{t}	0.34375
s	0.008 m	s*	1
$\{T_{\mathrm{g}}\}_{\mathrm{in}}$	298 K	$\{T^*_{\mathrm{g}}\}_{\mathrm{in}}$	0
T_{mold}	373 K	T^*_{mold}	1
$\{v_{\mathrm{g},x}\}_{\mathrm{in}}$	0.001–0.1 m/s	$\{v^*_{\mathrm{g},x}\}_{\mathrm{in}}$	0–0.05
$\{v_{\mathrm{g},y}\}_{\mathrm{in}}$	0	$\{\mathbf{v}^*_{\mathrm{g},y}\}_{\mathrm{in}}$	0
$\mathbf{v}_{\mathrm{g}}\|_{\mathrm{gt}} \cdot \mathbf{n}_{\mathrm{gt}}$	0–0.05 m/s	$\mathbf{v}^*_{\mathrm{g}}\|_{\mathrm{gt}} \cdot \mathbf{n}_{\mathrm{gt}}$	0–0.05
μ_{g}	0.20 N s/m^2	$\mu^*_{\mathrm{g}}(= 1/Re)$	0.236–23.6
ρ_{g}	1060 kg/m^3	ρ^*_{g}	1
ϕ	0.26–0.61	Not defined	–

2.2. Flow simulation

A finite element based multiphysics software FEMLab 3.0 [15] is used to solve the microscopic continuity, momentum, and energy equations for flow through the gap region for the geometry shown in Fig. 4 under steady-state conditions. The figure shows two unit cells: a target unit cell preceded by a precursor unit cell. Eqs. (10)–(12) are solved both in the precursor and target unit cells. The precursor unit cell is included to ensure that the inlet velocity and temperature profiles for the target unit cell are as real as possible. The interface between the two unit cells is used as an internal boundary condition. (The result at the outlet of the precursor unit cell is used to define the conditions at the inlet of the target unit cell.) The dimensionless inlet velocity is specified as unity and the dimensionless inlet temperature is specified as a zero in the precursor unit cell. The pressure at the outlet plane of the target unit cell is specified as zero. Symmetry boundary conditions (y direction velocity, y-derivatives of x and y direction velocities, and y-derivative of temperature, are put equal to zero) are used at the upper and lower surfaces of the unit cells in the gap phase. Normal heat and volume flux conditions as per Eqs. (13) and (14) are applied on tow surfaces. In the precursor unit cell, the energy and volume fluxes across the tow–gap interface are specified as zeros; this ensure that the inlet velocity and temperature profiles for the target unit cell does not change when the effect of varying the energy flux and volume flux is studied. Table 1 lists typical parameter values used in our simulation. Lagrange P2–P1 elements are used and a total of 2288[6] elements are created in the gap region of unit cells (part A of Fig. 5). Once the microscopic transport equations are solved, $K_{\mathrm{th},ij}$ is evaluated using the post processing techniques that enable integration of user-defined expressions involving dependent variables such as velocity components and temperature. (Parts B and C of Fig. 5 show typical velocity and temperature fields in the gap region.)

[6] 572 elements were shown to be adequate to obtain convergence in most cases, so our FEM mesh is over refined.

2.3. Estimating $\mathbf{K}_{th}$ for 2D flow in the unit cell

The thermal conductivity tensor $K_{\mathrm{th},ij}$ has a total of nine components in 3D. We will first identify its relevant components in the 2D flow of the idealized dual-scale porous medium.

Recognizing that $V = V_{\mathrm{g}}/\varepsilon_{\mathrm{g}}$, Eq. (7) can be rewritten (after modifying the last term on its RHS) as

$$\mathbf{K}_{\mathrm{th}} = k_{\mathrm{g}}\varepsilon_{\mathrm{g}}\boldsymbol{\delta} + \frac{k_{\mathrm{g}}}{V}\int_{A_{\mathrm{gt}}} \mathbf{n}_{\mathrm{gt}}\mathbf{b}\,\mathrm{d}A - \frac{\rho_{\mathrm{g}}C_{\mathrm{p,g}}}{V}\int_{V_{\mathrm{g}}} \hat{\mathbf{v}}_{\mathrm{g}}\mathbf{b}\,\mathrm{d}V \tag{16}$$

This equation in component form can be written as

$$K_{\mathrm{th},ij} = k_{\mathrm{g}}\varepsilon_{\mathrm{g}}\delta_{ij} + \frac{k_{\mathrm{g}}}{V}\int_{A_{\mathrm{gt}}} n_{\mathrm{gt},i}b_j\,\mathrm{d}A - \frac{\rho_{\mathrm{g}}C_{\mathrm{p,g}}}{V}\int_{V_{\mathrm{g}}} \hat{v}_{\mathrm{g},i}b_j\,\mathrm{d}V \tag{17}$$

where i and j take values x, y, or z in a Cartesian coordinate system.

As described earlier, we solved for temperature and velocity numerically within the gap region of the unit

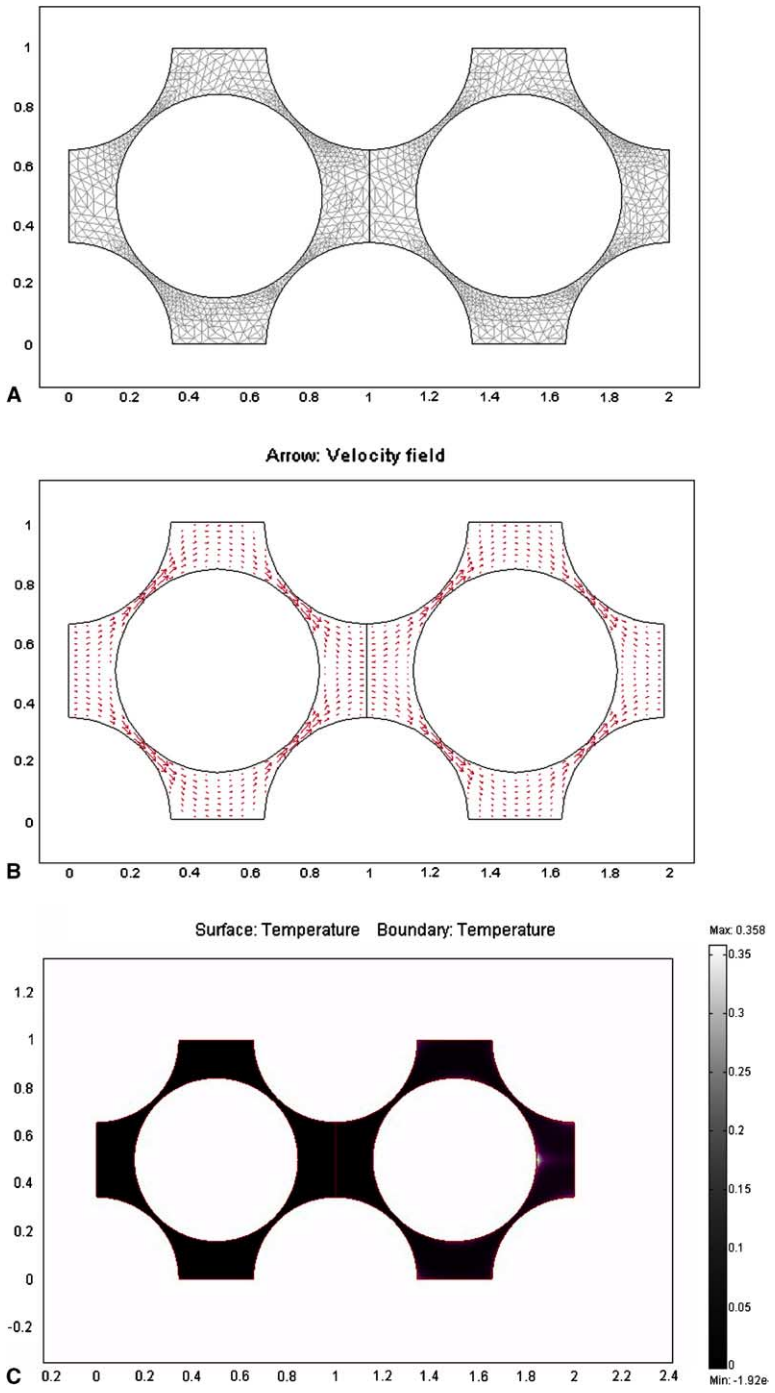

Fig. 5. Part (A): The FEM mesh used for flow simulations in the gap region; Part (B): Vector plot of a typical velocity field; Part(C): A typical temperature field.

cells. So it is only appropriate that we replace b_j with the temperature deviation term $\widehat{T}_g$ within the integrals so as to estimate $K_{th,ij}$. To that end, both sides of Eq. (16) are post-contracted with gradient of the gap-averaged temperature to yield

$$\mathbf{K}_{th} \cdot \nabla \langle T_g \rangle^g = k_g \varepsilon_g \nabla \langle T_g \rangle^g + \frac{k_g}{V} \int_{A_{gt}} \mathbf{n}_{gt} \widehat{T}_g \, dA - \frac{\rho_g C_{p,g}}{V} \int_{V_g} \hat{\mathbf{v}}_g \widehat{T}_g \, dV \tag{18}$$

In matrix form, this can be written as

$$\begin{bmatrix} K_{\mathrm{th},xx} & K_{\mathrm{th},xy} & K_{\mathrm{th},xz} \\ K_{\mathrm{th},yx} & K_{\mathrm{th},yy} & K_{\mathrm{th},yz} \\ K_{\mathrm{th},zx} & K_{\mathrm{th},zy} & K_{\mathrm{th},zz} \end{bmatrix} \begin{bmatrix} \partial\langle T_{\mathrm{g}}\rangle^{\mathrm{g}}/\partial x \\ \partial\langle T_{\mathrm{g}}\rangle^{\mathrm{g}}/\partial y \\ \partial\langle T_{\mathrm{g}}\rangle^{\mathrm{g}}/\partial z \end{bmatrix}$$
$$= k_{\mathrm{g}}\varepsilon_{\mathrm{g}} \begin{bmatrix} \partial\langle T_{\mathrm{g}}\rangle^{\mathrm{g}}/\partial x \\ \partial\langle T_{\mathrm{g}}\rangle^{\mathrm{g}}/\partial y \\ \partial\langle T_{\mathrm{g}}\rangle^{\mathrm{g}}/\partial z \end{bmatrix} + \frac{k_{\mathrm{g}}}{V} \begin{bmatrix} \int_{A_{\mathrm{gt}}} n_{\mathrm{gt},x}\widehat{T}_{\mathrm{g}}\,\mathrm{d}A \\ \int_{A_{\mathrm{gt}}} n_{\mathrm{gt},y}\widehat{T}_{\mathrm{g}}\,\mathrm{d}A \\ \int_{A_{\mathrm{gt}}} n_{\mathrm{gt},z}\widehat{T}_{\mathrm{g}}\,\mathrm{d}A \end{bmatrix}$$
$$- \frac{\rho_{\mathrm{g}}C_{\mathrm{p,g}}}{V} \begin{bmatrix} \int_{V_{\mathrm{g}}} \hat{v}_{\mathrm{g},x}\widehat{T}_{\mathrm{g}}\,\mathrm{d}V \\ \int_{V_{\mathrm{g}}} \hat{v}_{\mathrm{g},y}\widehat{T}_{\mathrm{g}}\,\mathrm{d}V \\ \int_{V_{\mathrm{g}}} \hat{v}_{\mathrm{g},z}\widehat{T}_{\mathrm{g}}\,\mathrm{d}V \end{bmatrix} \tag{19}$$

Consider the flow of resin along x direction in an idealized geometry of a dual-scale porous medium as shown in Fig. 5. The porous medium is periodic and is analyzed in terms of unit cells. The target unit cell is selected in an array of infinitely long cylindrical tows whose axes are oriented along the z direction and are periodically arranged in the x–y plane. The flow is taking place from left to right, and the macroscopic temperature gradient is applied in the same direction as well. A steady-state non-isothermal flow is created in the unit cell such that the $y = s/2$ plane passing through the center of the middle cylindrical tow is the plane of symmetry. For such a system, Eq. (19) simplifies to

$$\begin{bmatrix} K_{\mathrm{th},xx} & K_{\mathrm{th},xy} & 0 \\ 0 & K_{\mathrm{th},yy} & 0 \\ 0 & 0 & k_{\mathrm{g}}\varepsilon_{\mathrm{g}} \end{bmatrix} \begin{bmatrix} \partial\langle T_{\mathrm{g}}\rangle^{\mathrm{g}}/\partial x \\ 0 \\ 0 \end{bmatrix}$$
$$= k_{\mathrm{g}}\varepsilon_{\mathrm{g}} \begin{bmatrix} \partial\langle T_{\mathrm{g}}\rangle^{\mathrm{g}}/\partial x \\ 0 \\ 0 \end{bmatrix} + \frac{k_{\mathrm{g}}}{V} \begin{bmatrix} \int_{A_{\mathrm{gt}}} n_{\mathrm{gt},x}\widehat{T}_{\mathrm{g}}\,\mathrm{d}A \\ 0 \\ 0 \end{bmatrix}$$
$$- \frac{\rho_{\mathrm{g}}C_{\mathrm{p,g}}}{V} \begin{bmatrix} \int_{V_{\mathrm{g}}} \hat{v}_{\mathrm{g},x}\widehat{T}_{\mathrm{g}}\,\mathrm{d}V \\ 0 \\ 0 \end{bmatrix} \tag{20}$$

Details of simplifications of $K_{\mathrm{th},ij}$ are given in the Appendix.[7] Note that the y and z components of the last two vectors on the RHS of Eq. (19) go to zero due to (a) symmetry across the central plane $y = s/2$, and (b) disappearance of both $n_{\mathrm{gt},z}$ and $\hat{v}_{\mathrm{g},z}$, respectively.

Finally the simplification of Eq. (20) yields

$$K_{\mathrm{th},xx} = k_{\mathrm{g}}\varepsilon_{\mathrm{g}} + \frac{\frac{k_{\mathrm{g}}}{V}\int_{A_{\mathrm{gt}}} n_{\mathrm{gt},x}\widehat{T}_{\mathrm{g}}\,\mathrm{d}A}{\frac{\partial\langle T_{\mathrm{g}}\rangle^{\mathrm{g}}}{\partial x}} - \frac{\frac{\rho_{\mathrm{g}}C_{\mathrm{p,g}}}{V}\left(\int_{V_{\mathrm{g}}}\widehat{T}_{\mathrm{g}}\hat{v}_{\mathrm{g},x}\,\mathrm{d}V\right)}{\frac{\partial\langle T_{\mathrm{g}}\rangle^{\mathrm{g}}}{\partial x}} \tag{21}$$

This relevant thermal conductivity term after non-dimensionalization is given as

$$K^{*}_{\mathrm{th},xx} = \varepsilon_{\mathrm{g}} + \frac{\frac{1}{V^{*}}\int_{A^{*}_{\mathrm{gt}}} n_{\mathrm{gt},x}\widehat{T}^{*}_{\mathrm{g}}\,\mathrm{d}A^{*}}{\frac{\partial\langle T^{*}_{\mathrm{g}}\rangle^{\mathrm{g}}}{\partial x^{*}}} - \frac{\frac{C^{*}_{\mathrm{p,g}}}{V^{*}}\int_{V^{*}_{\mathrm{g}}}\widehat{T}^{*}_{\mathrm{g}}\hat{v}^{*}_{\mathrm{g},x}\,\mathrm{d}V^{*}}{\frac{\partial\langle T^{*}_{\mathrm{g}}\rangle^{\mathrm{g}}}{\partial x^{*}}} \tag{22}$$

(Note that division of Eq. (21) by k_{g} renders the whole equation dimensionless. So one may feel that evaluating $K^{*}_{\mathrm{th},xx}$ with the help of dimensionless quantities, as done in Eq. (22), is rather unnecessary. But since we are solving the dimensionless forms of the continuity, momentum and energy equations using FEMLab [15], the output is in terms of dimensionless variables as well–hence evaluation of $K^{*}_{\mathrm{th},xx}$ with the help of Eq. (22) is straightforward.)

3. Results and discussion

In this section, the results obtained from numerical simulations for the saturated region, where the absorption rate of resin by the tows is absent, is discussed first. In this region, only the energy flux across the tow–gap interface is present. This is followed by the results obtained for the unsaturated region where both energy and volume fluxes exist across the tow–gap interface.

3.1. Fully saturated dual-scale flow

The permeability of tows is many orders-of-magnitude smaller than that of the gap phase. As a result when the tows get fully saturated, most of the resin passes through the gaps and the sink term S computed through Eq. (4) can be assumed to be negligible. But if the tow and gap phases are not in thermal equilibrium, transfer of energy takes place across the tow–gap interface even though tows are not absorbing any resin[8] (see Fig. 1). The effect of this interfacial heat-flux on the effective thermal conductivity during the saturated flow regime through a dual-scale porous medium is studied here.

In Fig. 6, the xx component of the dimensionless effective thermal conductivity $K^{*}_{\mathrm{th},xx}$ is plotted as a function of dimensionless interfacial heat-flux at zero and

[7] It is to be noted that the effective thermal conductivity tensor need not be a symmetric tensor. This is because of the dyadic products within the second area integral and the third volume integral on the right hand side of Eq. (7)—seeking a transpose of $\mathbf{K}_{\mathrm{th}}$ will require switching the order of the two vectors constituting the two dyads and such 'switched' dyads will not be equal!

[8] This fact was observed by Jadhav and Pillai [17] as well during their simulation of the mold-filling process in a two-layered dual-scale porous medium.

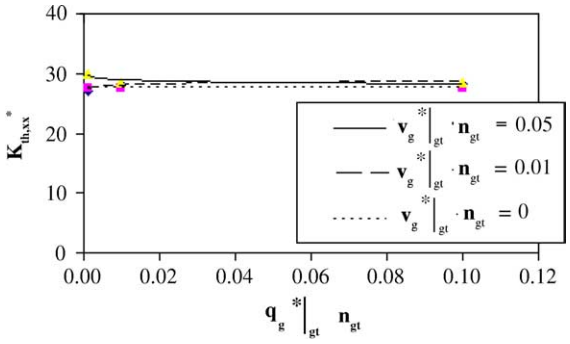

Fig. 6. Effect of interfacial heat-flux on the effective thermal conductivity at varying strengths of the sink effect.

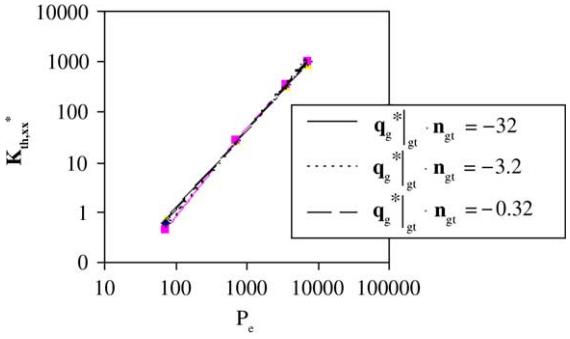

Fig. 7. Effect of Péclet number on the effective thermal conductivity at different interfacial heat-flux. Here the sink effect is zero (i.e. liquid absorption by tows is zero or $\mathbf{v}_g^*|_{gt} \cdot \mathbf{n}_{gt} = 0$).

non-zero sink terms (or interfacial volume fluxes). The plot indicates that $K^*_{th,xx}$ is independent of the interfacial heat-flux. This also suggests that the one single effective thermal conductivity can be used for the saturated region in the LCM mold irrespective of local thermal equilibrium between the tow and gap regions.

The focus is now turned towards studying the effect of increasing the unit cell inlet velocity on the effective thermal conductivity. Since the effective thermal conductivity depends on velocity deviations within the target unit cell through its dispersion component (third term in the RHS of Eq. (21)), the inlet velocity is expected to have a significant impact on its magnitude. In Fig. 7, the effect of increasing the inlet velocity on $K^*_{th,xx}$ is studied by plotting the conductivity against the Péclet number. As expected, the effective thermal conductivity increases as a function of Péclet number in the form of $K^*_{th,xx} \alpha Pe^{1.5}$.

3.2. Unsaturated dual-scale flow

In the unsaturated region behind the front as shown in Fig. 1, the resin seeps into the tows and give rise to the 'sink' effect mentioned with the equation of continuity (Eq. (3)). The sink term S, directly proportional to the interfacial volume flux, is governed by the liquid absorption rate of tows. In this section, we wish to study the effect of 'sink' phenomenon or the liquid absorption rate of tows on the effective thermal conductivity.

In addition to suggesting that the dimensionless effective thermal conductivity $K^*_{th,xx}$ in target unit cell is independent of the interfacial energy flux in the saturated region, Fig. 6 also suggests that this is true even in the unsaturated region as long as the inlet velocity does not change. Fig. 8 shows $K^*_{th,xx}$ as a function of Péclet number at different interfacial volume flux and at a constant interfacial heat-flux. The plot suggests that $K^*_{th,xx}$ continues to be a strong of function of Péclet number but is independent of absorption rate of resin at a given interfacial energy flux. In Fig. 9, the ratio of $K^*_{th,xx}$ at a given interfacial volume transfer rate and at zero rate is plotted as a function of Péclet number to capture the nuances missed by Fig. 8. The plot indicates that the effective thermal conductivity increases at a slightly faster rate at higher interfacial volume transfer rates.

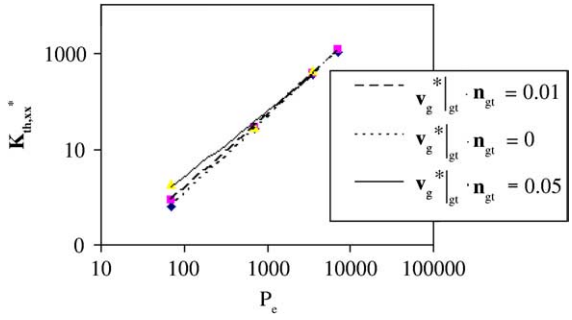

Fig. 8. Effect of Péclet number on the effective thermal conductivity at varying strengths of the sink effect. Here the interfacial heat-flux $\mathbf{q}_g^*|_{gt} \cdot \mathbf{n}_{gt} = -3.2$.

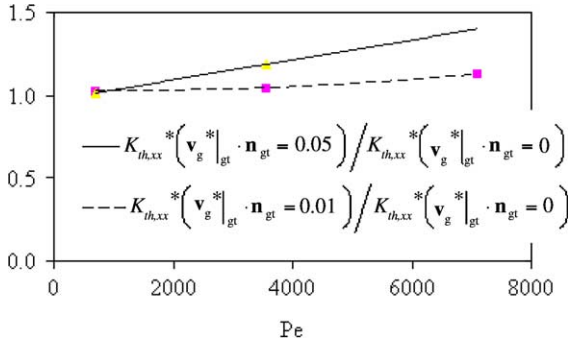

Fig. 9. Effect of Péclet number on the ratio of effective thermal conductivities at finite and zero sink strengths or interfacial absorption rates.

The observations drawn from Figs. 6, 8 and 9 have some potentially useful implications. One can conclude that the effective thermal conductivity term is a function of Péclet number and is independent of either the resin absorption rate by tows (the 'sink' effect) or the energy flux from tows into the gap region.

3.3. Effect of gap fraction on $K_{th,xx}$

Since the extent of the gap region is expected to influence the temperature and velocity distributions (and hence the dimensionless effective thermal conductivity $K^*_{\mathrm{th},xx}$), the simulations are carried out at three different gap fractions (ε_g) to study the effect of the inter-tow spacing in a dual-scale medium on $K^*_{\mathrm{th},xx}$.

Fig. 10 shows the effect of the resin absorption rate by tows on $K^*_{\mathrm{th},xx}$ at ε_g of 26%, 40%, and 61%; it is evident that the $K^*_{\mathrm{th},xx}$ is only a weak function of the resin absorption rates. Further, it appears that $K^*_{\mathrm{th},xx}$ can either increase or decrease with an increase in the absorption rate depending on the structure and porosity of the gap region. This increase or decrease in the effective thermal conductivity is primarily driven by the dispersion term. Taking a closer look at the dispersion (third) term in Eq. (21) reveals that the integrand is a product of deviations of the local temperature and velocity, with denominator as the gradient of the gap-averaged temperature. When the resin absorption rate increases, the average velocity at the outlet of the target unit cell decreases, and the average outlet temperature increases, resulting in an increase in both the velocity and temperature deviation terms. The effect of absorption rate on $K^*_{\mathrm{th},xx}$ depends on whether the integral of the product of both these deviations increases faster or slower than the temperature gradient.

Fig. 11 plots $K^*_{\mathrm{th},xx}$ as a function of the gap–tow interfacial heat-flux. Clearly, the effective thermal conductivity is independent of the heat-flux at all three gap fractions.

Both Figs. 10 and 11 indicate that $K^*_{\mathrm{th},xx}$ is a strong function of the gap fraction ε_g. Since ε_g is related to gap volume within the target unit cell, one can surmise

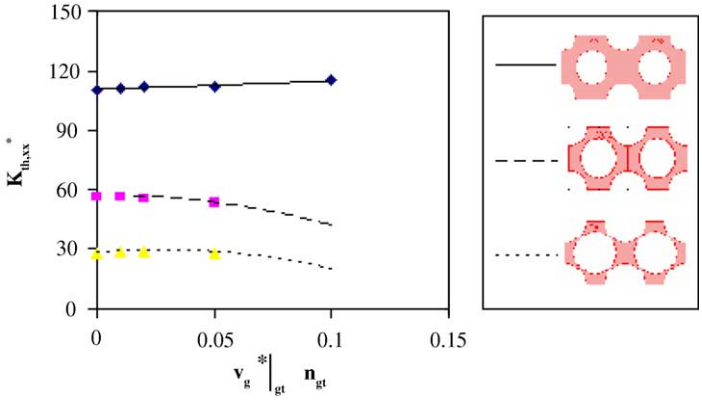

Fig. 10. Effect of absorption rate on the effective thermal conductivity at different gap fractions ($\varepsilon_g = 0.61, 0.40, 0.26$). Here the interfacial heat-flux $\mathbf{q}^*_g|_{gt} \cdot \mathbf{n}_{gt} = -3.2$.

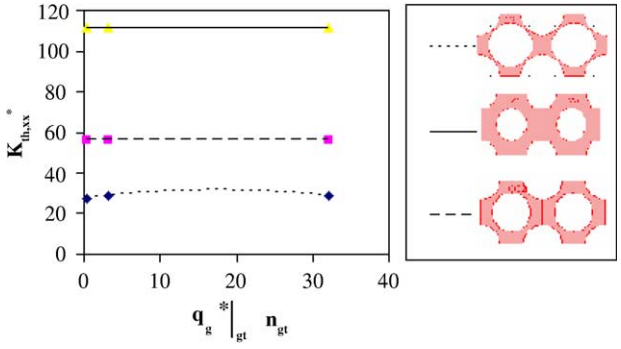

Fig. 11. Effect of heat-flux on the effective thermal conductivity at different porosities ($\varepsilon = 0.61, 0.40, 0.26$). $\mathbf{v}^*_g|_{gt} \cdot \mathbf{n}_{gt} = 0.01$.

that the effective thermal conductivity increases rather strongly with an increase in spacing between tows.

4. Conclusions

Variations in the relevant xx component of the effective thermal conductivity of a dual-scale porous medium were successfully estimated using a 2D non-isothermal flow simulation in a unit cell. Numerical predictions revealed some unexpected and potentially useful insights into how the effective thermal conductivity responds to changes in the inlet velocity, interfacial volume flux from gaps into tows, interfacial energy flux from tows into the gap phase, and spacing between tows. Neither the resin absorption rate nor the energy flux across the tow–gap interface seems to have a significant effect on the effective thermal conductivity of resin in gap phase. This implies that the effective thermal conductivity measured for the saturated flow in a dual-scale porous medium can perhaps be applied to the unsaturated region behind the flow front as well. Moreover in the saturated region, the effective thermal conductivity is indifferent to the presence or absence of local thermal equilibrium between tows and gaps. Predictably, an increase in spacing between tows leads to an increase in the effective thermal conductivity.

4.1. Limitations and future work

The current work aims to estimate the relevant xx component of the effective thermal conductivity tensor of a dual-scale porous media during the saturated and unsaturated flow.

But it fails to tell us anything about the other components or the invariants of the tensor. We would like to explore if those other components can be estimated under other ideal flow conditions in a unit cell under different boundary conditions. The present work treats liquid absorption flux and heat release flux on tow surfaces as parameters; in a real mold-filling situations, these quantities are changing rapidly with time during the unsaturated flow and are governed by flow conditions inside and outside the tows. So perhaps a more involved transient flow simulation with interfacial flux changing with time in a highly non-linear manner is needed to study the evolution of $K_{\mathrm{th},xx}$ during the unsaturated flow.

Acknowledgement

We gratefully acknowledge the financial support provided by TTTP program of CTS division of National Science Foundation in the form of CAREER research grant (# 0348097), as well as the financial support extended by S.C. Johnson & Son, Inc.

Appendix A. Simplified effective thermal conductivity tensor for flow perpendicular to periodically placed cylindrical tows

This appendix shows how each of the components of the average effective thermal conductivity tensor simplifies for flow of resin across tows as shown in Fig. 5 by evaluating Eq. (17) which is reproduced here for completeness.

$$K_{\mathrm{th},ij} = k_{\mathrm{g}}\varepsilon_{\mathrm{g}}\delta_{ij} + \frac{k_{\mathrm{g}}}{V}\int_{A_{\mathrm{gt}}} n_{\mathrm{gt},i} b_j \,\mathrm{d}A - \frac{\rho_{\mathrm{g}} C_{\mathrm{p,g}}}{V}\int_{V_{\mathrm{g}}} \hat{v}_{\mathrm{g},i} b_j \,\mathrm{d}V \tag{A.1}$$

Since the pressure gradient is applied in the x direction and the axis of the cylindrical tows coincides with z direction, the normal vector at the tow–gap interface does not have a z component. In addition, the velocity vector of the resin in the gap phase does not have a z component either. Thus both $n_{\mathrm{gt},z}$ and $\hat{v}_{\mathrm{g},z}$ are identically equal to zero and hence $K_{\mathrm{th},zx}$ and $K_{\mathrm{th},zy}$ vanish, and $K_{\mathrm{th},zz}$ becomes a constant of value $k_{\mathrm{g}}\varepsilon_{\mathrm{g}}$. Because of lack of change along the z direction, the temperature remains constant in this direction implying that the temperature deviation in the z direction is zero. Hence the term b_z is zero and as a result, both $K_{\mathrm{th},xz}$, and $K_{\mathrm{th},yz}$ reduce to zero. The remaining terms of the average effective thermal conductivity tensor are shown below.

$$K_{\mathrm{th},xx} = k_{\mathrm{g}}\varepsilon_{\mathrm{g}} + \frac{k_{\mathrm{g}}}{V}\int_{A_{\mathrm{gt}}} n_{\mathrm{gt},x} b_x \,\mathrm{d}A - \frac{\rho_{\mathrm{g}} C_{\mathrm{p,g}}}{V}\int_{V_{\mathrm{g}}} \hat{v}_{\mathrm{g},x} b_x \,\mathrm{d}V \tag{A.2}$$

$$K_{\mathrm{th},xy} = \frac{k_{\mathrm{g}}}{V}\int_{A_{\mathrm{gt}}} n_{\mathrm{gt},x} b_y \,\mathrm{d}A - \frac{\rho_{\mathrm{g}} C_{\mathrm{p,g}}}{V}\int_{V_{\mathrm{g}}} \hat{v}_{\mathrm{g},x} b_y \,\mathrm{d}V \tag{A.3}$$

$$K_{\mathrm{th},yx} = \frac{k_{\mathrm{g}}}{V}\int_{A_{\mathrm{gt}}} n_{\mathrm{gt},y} b_x \,\mathrm{d}A - \frac{\rho_{\mathrm{g}} C_{\mathrm{p,g}}}{V}\int_{V_{\mathrm{g}}} \hat{v}_{\mathrm{g},y} b_x \,\mathrm{d}V \tag{A.4}$$

$$K_{\mathrm{th},yy} = k_{\mathrm{g}}\varepsilon_{\mathrm{g}} + \frac{k_{\mathrm{g}}}{V}\int_{A_{\mathrm{gt}}} n_{\mathrm{gt},y} b_y \,\mathrm{d}A - \frac{\rho_{\mathrm{g}} C_{\mathrm{p,g}}}{V}\int_{V_{\mathrm{g}}} \hat{v}_{\mathrm{g},y} b_y \,\mathrm{d}V \tag{A.5}$$

Both integral terms on the RHS of the Eq. (A.2) are not identically equal to zero and hence $K_{\mathrm{th},xx}$ is not a simple constant. In the target unit cell, each point in the lower half of the unit cell has a mirror image across the plane of symmetry $y = s/2$, and both these points have the same value of $\hat{T}_{\mathrm{g}}$ (equivalently have same b_x as the temperature gradient vector is along the x direction only), and equal and opposite values of $n_{\mathrm{gt},y}$ and $\hat{v}_{\mathrm{g},y}$. As a result, the terms $\int_{A_{\mathrm{gt}}} n_{\mathrm{gt},y} b_x \,\mathrm{d}A$ and $\int_{V_{\mathrm{g}}} \hat{v}_{\mathrm{g},y} b_x \,\mathrm{d}V$ are identically equal to zero, and hence $K_{\mathrm{th},yx}$ is also zero. Since b_y can be evaluated only when the volume-averaged temperature gradient is applied along the y direction, nothing can be said about the $K_{\mathrm{th},xy}$ and $K_{\mathrm{th},yy}$ as both these components contain the indeterminate b_y because the volume-averaged temperature gradient exists only along the x direction. In any case, as the temperature gradient

does not exist in the y direction, the magnitudes of both these components do not have any bearing on the energy equation and hence do not hinder our analysis in anyway.

So the final effective thermal conductivity tensor in matrix form is

$$\mathbf{K}_{\mathrm{th}} = \begin{bmatrix} K_{\mathrm{th},xx} & K_{\mathrm{th},xy} & 0 \\ 0 & K_{\mathrm{th},yy} & 0 \\ 0 & 0 & k_{\mathrm{g}}\varepsilon_{\mathrm{g}} \end{bmatrix} \tag{A.6}$$

References

[1] C.D. Rudd, A.C. Long, K.N. Kendall, C.G.E. Mangin, Liquid Molding Technologies, Woodhead, 1997.

[2] B.Z. Babu, K.M. Pillai, Experimental investigation of the effect of fiber-mat architecture on the unsaturated flow in liquid composite molding, J. Comp. Mater. 38 (1) (2004) 57–79.

[3] S. Whitaker, The Method of Volume Averaging, Kluwer Academi, Dordrecht, 1999.

[4] M. Kaviany, Principles of Heat Transfer in Porous Media, second ed., Springer, New York, 1995.

[5] C.L. Tucker III, R.B. Dessenberger, Governing equations for flow and heat transfer in stationary fiber beds, in: S.G. Advani (Ed.), Flow and Rheology in Polymer Composites Manufacturing, Elsevier, Amsterdam, 1994.

[6] J. Bear, Y. Bachmat, Introduction to Modeling of Transport Phenomena in Porous Media, Kluwer, Dordrecht, 1990.

[7] J.C. Slattery, Single-phase flow through porous media, Am. Inst. Chem. Eng. 15 (6) (1969) 866–872.

[8] W.G. Gray, P.C.Y. Lee, On the theorems for local volume averaging of multiphase systems, Int. J. Multiphase Flow 3 (1977) 333–340.

[9] S. Whitaker, Flow in porous media, I. A theoretical derivation of Darcy's law, Transport Porous Media 1 (1986) 3–25.

[10] K. O'Neil, G.F. Pinder, A derivation of equations for transport of liquid and heat in three dimensions in a fractured porous medium, Adv. Water Resour. 4 (1981) 150–164.

[11] S.M. Hassanizadeh, Modeling species transport by concentrated brine in aggregated porous media, Transport Porous Media (3) (1988) 299–318.

[12] K.M. Pillai, Governing equations for unsaturated flow through woven fiber mats: Part1 Isothermal flows, Comp. Part A: Appl. Sci. Manufact. 33 (2002) 1007–1019.

[13] K.M. Pillai, M.S. Munagavalasa, Governing equations for unsaturated flow through woven fiber mats, Part2: Non-isothermal reactive flows, Comp. Part A: Appl. Sci. Manufact. 35 (2004) 403–415.

[14] K.T. Hsiao, S.G. Advani, Modified effective thermal conductivity due to heat dispersion in fibrous porous media, Int. J. Heat Mass Transfer 42 (1999) 1237–1254.

[15] Comsol, Inc., 1100 Glendon avenue, 17th floor, Los Angeles, CA 90024. FEMLab 3 user's guide, version: January 2004.

[16] K.M. Pillai, S.G. Advani, A model for unsaturated flow in woven or stitched fiber mats during mold filling in resin transfer molding, J. Comp. Mater. 32 (19) (1998) 1753–1783.

[17] S.R. Jadhav, K.M. Pillai, Numerical study of heat transfer during unsaturated flow in dual-scale porous media, Numer. Heat Transfer, Part A 43 (2003) 385–407.